

## Article

# Use of Vine Shoot Waste for Manufacturing Innovative Reinforced Cement Composites

Daniela Alexandra Scurtu <sup>1,\*</sup>, Eniko Kovacs <sup>1,2</sup>, Lacrimioara Senila <sup>1</sup>, Erika Andrea Levei <sup>1</sup>, Dorina Simedru <sup>1</sup>, Xenia Filip <sup>3</sup>, Monica Dan <sup>3</sup>, Cecilia Roman <sup>1</sup>, Oana Cadar <sup>1,\*</sup> and Leontin David <sup>1,4</sup>

<sup>1</sup> Research Institute for Analytical Instrumentation, Research Institute for Analytical Instrumentation Subsidiary, National Institute for Research and Development for Optoelectronics INOE 2000, 67 Donath Street, 400293 Cluj-Napoca, Romania

<sup>2</sup> Faculty of Horticulture, University of Agricultural Sciences and Veterinary Medicine, 3-5 Manastur Street, 400372 Cluj-Napoca, Romania

<sup>3</sup> National Institute for Research and Development of Isotopic and Molecular Technologies, 67-103 Donath Street, 400293 Cluj-Napoca, Romania

<sup>4</sup> Faculty of Physics, Babes-Bolyai University, 1 Mihail Kogalniceanu Street, 400084 Cluj-Napoca, Romania

\* Correspondence: daniela.scurtu@icia.ro (D.A.S.); oana.cadar@icia.ro (O.C.)

**Abstract:** Due to the current concern with the environmental impacts produced by the construction industry, many studies have been conducted to capitalize on the advantages of waste to develop sustainable materials. The study reports an innovative, non-conventional cement-based composite material containing 10 wt.% vine shoot waste, representing a step forward toward the use of this lignocellulosic waste. The investigations were carried out using scanning electron microscopy with energy dispersive X-ray analysis, Fourier-transform infrared spectroscopy, thermogravimetric analysis, X-ray diffraction and solid-state <sup>27</sup>Al and <sup>29</sup>Si nuclear magnetic resonance spectroscopy. The addition of vine shoot waste to the cement paste increases the amount of hydration products (calcium silicate hydrate (CSH), calcium hydroxide (CH), calcium carbonate (CaCO<sub>3</sub>) and ettringite), leading to a more compact and dense structure. The structural characterization techniques also confirmed the formation of a higher amount of hydration products in the case of vine shoot waste added to the cement paste.

**Keywords:** vine shoot waste; cement paste; structural properties; hydration products; NMR spectroscopy



**Citation:** Scurtu, D.A.; Kovacs, E.; Senila, L.; Levei, E.A.; Simedru, D.; Filip, X.; Dan, M.; Roman, C.; Cadar, O.; David, L. Use of Vine Shoot Waste for Manufacturing Innovative Reinforced Cement Composites. *Appl. Sci.* **2023**, *13*, 134. <https://doi.org/10.3390/app13010134>

Academic Editor: Ana Paula Betencourt Martins Amaro

Received: 5 December 2022

Revised: 13 December 2022

Accepted: 20 December 2022

Published: 22 December 2022



**Copyright:** © 2022 by the authors. Licensee MDPI, Basel, Switzerland. This article is an open access article distributed under the terms and conditions of the Creative Commons Attribution (CC BY) license (<https://creativecommons.org/licenses/by/4.0/>).

## 1. Introduction

Cement is one of the most widely used materials in the construction industry [1]. The cement industry is responsible for approximately 8% of global anthropogenic carbon dioxide emissions, making it an important sector for carbon dioxide-emission mitigation approaches [2,3]. The EN 197-1 standard defines the specifications of 27 common types of cement, including 7 sulfate-resistant types of cement, 3 low early-resistance blast-furnace types of cement and 2 with high sulfate resistance [4]. Portland type I (CEM I) cement is suitable for general use (bridges, buildings, reservoirs, pipe and pre-cast concrete products), where the special properties of other cement types are not required.

The composition of CEM I is 95–100 wt.% clinker and 0–5 wt.% additional constituents, while the white CEM I contains 51–72 wt.% tricalcium silicate (C<sub>3</sub>S), 9–25 wt.% dicalcium silicate (C<sub>2</sub>S), 5–13 wt.% tricalcium aluminate (C<sub>3</sub>A) and 1–2 wt.% tetracalcium iron aluminate (C<sub>4</sub>AF). Cement hydration is an irreversible and complex chemical reaction between cement and water, resulting in different hydration products such as calcium silicate hydrate (CSH), calcium aluminoferrite hydrate, ettringite, trisulfoaluminate, monosulfoaluminate and other related compounds [5].

Anthropogenic activities generate large amounts of waste, which is a significant concern for environmental protection; the impact can be reduced by reasonable waste control [6]. Approximately 50 million cubic meters of agricultural waste are produced yearly in the European Union due to agricultural activities and various industries, such as forestry and furniture manufacturing [7,8]. Improved waste management through using waste in various domains as alternative raw materials contributes to reducing greenhouse gas emissions [9]. Recent research has focused on converting waste into valuable products [10]. In this regard, fusing glass powder waste to improve the mechanical properties of cementitious materials is both cost-effective and environmentally friendly [11]. Moreover, the mechanical properties of cement-based materials can be improved using granite cutting residue [12]. The addition of red mud to magnesium phosphate cement resulted in higher fluidity and improved mechanical properties and water resistance [13]. Additionally, the partial replacement of Portland cement with volcanic ash provides a low-cost and environmentally friendly solution to the disposal of volcanic ash [14].

Lignocellulosic waste can be used in cement-based materials as alternative raw material that positively impacts the cement-based structure [15,16]. Due to the lignocellulosic fiber malleability and morphology, adding waste to cement-based materials improves the compatibility between fiber and matrix and thus yields enhanced flexural and tensile strength, lightweight properties, ductility, cracks and fractures of cement-based materials [17]. The increased surface area of the lignocellulosic waste increases the water absorption of the composite cement-based material [18]. The main factors affecting the quality of composite cement-based materials are density, particle size, lignocellulosic material type, aspect ratio, volume, mix design, and the method used for mixing, processing and curing, respectively [15]. Low lignin content offers high hydrophilicity due to the only two free hydroxyl groups, compared with cellulose with three free hydroxyl groups. In addition, using lignocellulosic waste with a low affinity for water might avoid degradation caused by alkaline pore water in cement-based materials [19].

A cement-bonded panel was constructed using pine shavings, sugar cane bagasse particles, eucalyptus, Pinus and bamboo lamination residues [20]. The genus Pinus is the conifer species most widely used cement-based material. Adding Pinus wood residue increases the material's physical properties associated with the particle size. A possible explanation could be that smaller particles are coated better with cement and provide better bonding [21,22]. Using coir fiber reinforcement in masonry mortar materials results in lower densities. The lignocellulosic fragments with shorter lengths are better for reinforcement, and the water absorption capacity of 15% decreases with the fiber size [23]. Karade et al. reported using various lignocellulosic wastes (rice straw, hazelnut shell, coir, oil palm residues, wheat straw, bark, bagasse, corn granules and achar stalks) in construction. The advantages of their use are the reduction of carbon dioxide emissions, safe and efficient waste disposal, low thermal conductivity, enhanced bio and fire resistance and a lightweight composite cement-based material [15].

Vine shoot waste (VSW) is another type of lignocellulosic biomass generated in large quantities worldwide and is commonly burned on the field or used as compost [24,25]. To the best of our knowledge, apart from studies conducted on the use of vine shoot waste as a source of bioenergy [26], cellulose nanocrystals [27], particleboards [28] and clay bricks [29], no such renewable raw material has previously been used to enhance the properties of cement. In this regard, the study aims to obtain an innovative cement-based material by adding 10 wt.% vine shoot waste. Thermogravimetric analysis (TGA), X-ray diffraction (XRD), scanning electron microscopy with energy dispersive X-ray analysis (SEM-EDX), Fourier-transformed infrared (FT-IR) spectroscopy and solid-state <sup>27</sup>Al and <sup>29</sup>Si nuclear magnetic resonance (NMR) spectroscopy evidenced the improved structural and hydration properties of the cement paste with 10 wt.% vine shoot waste. The obtained results contribute to the enhancement of knowledge in the field of waste management and the progress toward the circular economy by providing sustainable ways of waste disposal.

## 2. Materials and Methods

This section is focused on the presentation of raw materials and the determination methods used for the chemical and structural characterization of the cement (CEM), vine shoot waste (VSW), cement paste (CP), and cement paste 10% vine shoot waste (CP10VSW) samples.

### 2.1. Chemicals and Raw Materials

All chemicals (Merck, Darmstadt, Germany) used in this study were of analytical grade and used as received without any further purification. For the production of the lignocellulosic waste cement composites, the following materials were used: cement (CEM, Figure 1a) and vine shoot waste (VSW, Figure 1b). The white cement CEM I 52.5 R used in this study is an ordinary Portland cement type I containing 63 wt.% tricalcium silicate ( $C_3S$ ), 18 wt.% dicalcium silicate ( $C_2S$ ), 10 wt.% tricalcium aluminate ( $C_3A$ ) and 1 wt.% tetracalcium iron aluminate ( $C_4AF$ ), according to the producer. VSW was procured from “Ion Ionescu de la Brad” research station of the University of Agricultural Sciences, Iasi. The vine shoot waste was dried at 105 °C and ground to <100 µm.

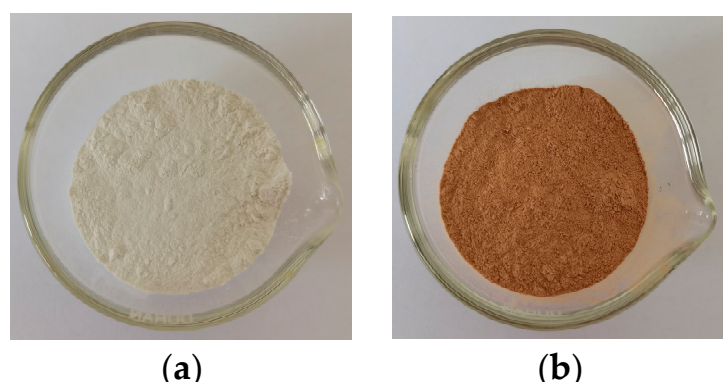


**Figure 1.** Images of (a) CEM and (b) VSW samples.

### 2.2. Vine Shoot Waste Cement Nanocomposite Production

An amount of 10 wt.% VSW was mixed with CEM for 1 min using an electric hand mixer with a rotation speed of 600 rpm. After adding water (water to cement ratio of 0.5), the mixing process continued for another 5 min. The cement paste containing VSW (CP10VSW) was cast in a cylindrical plastic mold with a diameter of 50 mm and a height of 100 mm and was sealed for the first 24 h. Afterward, the sample was demolded and immersed in distilled water for 28 days, oven dried at 100 °C for 4 h, followed by grinding (Figure 2a). A plain cement paste (CP) prepared similarly was used as a control sample (Figure 2b).

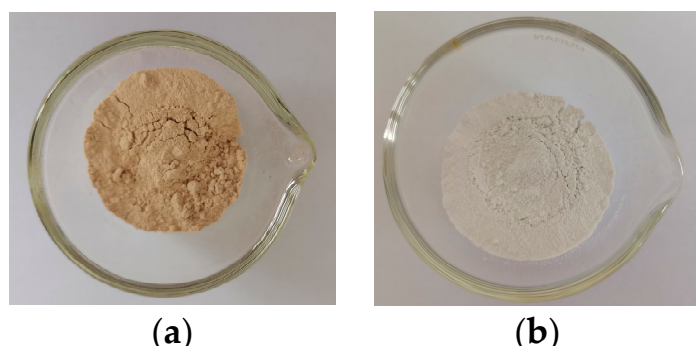


**Figure 2.** Images of (a) CP10VSW and (b) CP samples.

### 2.3. Chemical Characterization of Vine Shoot Waste

The following chemical characteristics were evaluated for the VSW sample used in this study: lignocellulosic components (cellulose, hemicelluloses, and lignin), moisture, C, H, N, S and ash contents. The cellulose and hemicellulose content of the dried VSW sample was determined from holocellulose content as the residues insoluble in NaOH [30]. The lignin content was determined as an insoluble residue after the reaction with H<sub>2</sub>SO<sub>4</sub>. Moisture content was determined according to EN ISO 18134-3 and refers to the sample dried at 105 °C in air atmosphere until the constant mass is achieved and the percentage moisture is calculated from the loss in mass of the biomass [31]. The total C, H, N, and S content were measured using a Flash 2000 CHNS/O analyzer (Thermo Fisher Scientific, Waltham, MA, USA). The ash content was determined according to the ASTM E1755-01 standard and refers to the inorganic residue remaining after the complete oxidation at 575 ± 25 °C of the organic matter in the vine shoot waste [32].

### 2.4. Chemical Characterization of Cement

For the cement (CEM) sample used in this study, the following chemical characteristics were evaluated: major elements (Si, Al, Fe, Na, K, Ca, Mg), oxides (Na<sub>2</sub>O, K<sub>2</sub>O, CaO, SiO<sub>2</sub>, Al<sub>2</sub>O<sub>3</sub>, Fe<sub>2</sub>O<sub>3</sub>) and loss of ignition (LOI). The major elements (Si, Al, Fe, Na, K, Ca, Mg) were determined using an Optima 5300 DV (Perkin Elmer, Norwalk, CT, USA) inductively-coupled plasma optical emission spectrometer (ICP-OES), after microwave digestion using the method previously described [33]. The calibration curves were prepared using 1000 mg/L multi-element (Al, Fe, Na, K, Ca, Mg) and mono-element standard (Si) solutions (Merck, Darmstadt, Germany). The measured element concentrations were converted to oxides using atomic and molecular masses. Loss on ignition (LOI) in the cement industry commonly refers to a mass loss for a sample heated to 1000 °C, determined according to ASTM C 114 [34]. A potash feldspar (BCS-CRM 376/1, Bureau of Analyzed Samples, Middlesbrough, UK) certified reference material with a similar matrix to the cement sample was analyzed for quality control. The obtained results (Na<sub>2</sub>O, K<sub>2</sub>O, CaO, SiO<sub>2</sub>, Al<sub>2</sub>O<sub>3</sub>, Fe<sub>2</sub>O<sub>3</sub>, LOI) for the certified reference feldspar material were in good agreement with the certified values.

### 2.5. Structural Characterization

The CEM, VSW, CP and CP10VSW samples were characterized in terms of thermal stability (TGA) and structural properties (XRD, SEM, FT-IR and NMR). The thermal stability of the CEM, VSW, CP, and CP10VSW samples was investigated using a thermogravimetric analysis instrument Q600 ADT (TA Instruments, New Castle, DE, USA) by heating from 30 to 1000 °C, with a heating rate 10 °C/min under air. The XRD patterns were recorded at room temperature using a D8 Advance diffractometer (Bruker, Karlsruhe, Germany) with CuK α1 radiation ( $\lambda = 1.54060 \text{ \AA}$ ), operating at 40 kV and 35 mA. SEM-EDX analysis was performed at room temperature using a scanning electron microscope (VEGAS 3 SBU, Tescan, Brno-Kohoutovice, Czech Republic) with a Quantax EDX XFlash (Bruker, Karlsruhe, Germany) detector. Samples of ~4 mm<sup>2</sup> were mounted with carbon tape to an SEM stub. The FT-IR spectra of CEM, VSW, CP and CP10VSW were recorded using a Spectrum BX II (Perkin Elmer, Waltham, MA, USA) spectrometer in the range of 4000–400 cm<sup>-1</sup> on 1% KBr pellets with a spectral resolution of 2 cm<sup>-1</sup>. <sup>29</sup>Si and <sup>27</sup>Al MAS (magic angle spinning) NMR spectra were recorded on a 500 MHz Bruker Advance III (Bruker, Billerica, MA, USA) solid-state wide-bore spectrometer, operating at <sup>29</sup>Si and <sup>27</sup>Al Larmor frequencies of 99.36 and 130.32 MHz, respectively. A 4 mm Bruker MAS probe was used, and the samples were taken in ZrO<sub>2</sub> rotors, which were spun at a rate of 7 kHz (for <sup>29</sup>Si spectra) and 14 kHz (for <sup>27</sup>Al spectra). The <sup>29</sup>Si MAS NMR spectra were recorded using one-pulse with a proton high power decoupling sequence with a relaxation delay of 5s, collecting 5000 FIDs for CEM and CP and 15000 FIDs for VSW and CP10VSW. These spectra were calibrated to tetramethylsilane (TMS) through an indirect procedure that uses sodium-3-(trimethylsilyl)-propane-1-sulfonate (DSS) (1.46 ppm) as an external reference. The <sup>27</sup>Al MAS NMR spectra

were recorded with one pulse sequence, accumulating 5000 FIDs with a relaxation delay of 1 s. The  $^{27}\text{Al}$  spectra were calibrated to the Al's signal ( $\delta = 0$  ppm) in an external standard 1M  $\text{Al}(\text{NO}_3)_3$  aqueous solution.

### 3. Results and Discussion

The chemical, structural, and hydration properties of the cement paste with 10 wt.% vine shoot waste (CP10VSW) sample were investigated by thermogravimetric analysis (TGA), X-ray diffraction (XRD), scanning electron microscopy with energy dispersive X-ray analysis (SEM-EDX), Fourier-transformed infrared (FT-IR) spectroscopy and solid-state  $^{27}\text{Al}$  and  $^{29}\text{Si}$  nuclear magnetic resonance (NMR) spectroscopy.

#### 3.1. Chemical Characterization

The chemical characterization of the vine shoot waste (VSW) sample used for the preparation of CP10VSW composite is presented in Table 1, and confirms the presence of cellulose, hemicellulose and lignin in comparable amounts, while the elemental analysis reveals a high C amount which is a constituent part of lignin. The higher amount of lignin in vine shoot waste makes it sustainable for cement paste due to the low affinity to water. The content of lignocellulosic constituents and elemental analysis is similar to those obtained in our previous studies for eight vine shoot waste varieties [35].

**Table 1.** Chemical composition (%) of the vine shoot waste (VSW) sample.

VSW	Amount (%)	VSW	Amount (%)
Lignocellulosic components	Elemental analysis		
Cellulose	$35.05 \pm 0.30$	N	$0.78 \pm 0.01$
Hemicelluloses	$26.40 \pm 0.20$	C	$46.7 \pm 1.50$
Lignin	$30.10 \pm 0.23$	H	$5.79 \pm 0.2$
Moisture	$7.90 \pm 0.02$	S	$0.19 \pm 0.01$
		Ash	$2.04 \pm 0.02$

#### 3.2. Chemical Characterization of Cement

The chemical characterization of the cement (CEM) sample used for preparing the CP10VSW composite confirms that CEM is composed of cement clinker and minor additional constituents. Its main components are dicalcium silicate ( $\text{C}_2\text{S}$ ), tricalcium aluminate ( $\text{C}_3\text{A}$ ), tricalcium silicate ( $\text{C}_3\text{S}$ ), and tetracalcium iron aluminate ( $\text{C}_4\text{AF}$ ). The experimental composition of cement used in this study (65.20 wt.%  $\text{CaO}$ , 21.73 wt.%  $\text{SiO}_2$ , 4.63 wt.%  $\text{Al}_2\text{O}_3$ , 0.45 wt.%  $\text{Fe}_2\text{O}_3$ , 1.00 wt.%  $\text{MgO}$ , 0.36 wt.%  $\text{Na}_2\text{O}$ , 0.14 wt.%  $\text{K}_2\text{O}$ , 3.00 wt.%  $\text{SO}_3$  and loss of ignition is 0.1 wt.%) was in accordance with the EN 197-1 and EN 196-2 standards [4,36]. These components highly influence the performance stability of cement and its products.

#### 3.3. Thermogravimetric Analysis (TGA)

The TGA curves of CEM, CP, CP10VSW and VSW samples are presented in Figure 3a–d. The TGA curve of the CEM sample (Figure 3a) displays three peaks at 109, 387, and 649 °C attributed to gypsum plaster dehydration, CH, and  $\text{CaCO}_3$ , respectively [37]. The TGA curves of the CP (Figure 3b) and CP10VSW (Figure 3c) samples display three distinct effects: (i) the exothermic effect at 100–400 °C corresponds to the removal of water from hydrated products, which are likely to include most cement phases, most of the CSH; (ii) the exothermic effect at 500–570 °C corresponds to the dehydroxylation of a part from CH [38,39]; (iii) the exothermic effect at 700–900 °C may be due to the decalcification of the  $\text{CaCO}_3$  [40]. Around 800 °C, the weight loss due to carbon dioxide elimination by thermal degradation of the carbonated phase is observed [41]. The TGA curve of the VSW sample (Figure 3d) reveals a slight weight loss due to the water removal at 100 °C, while the peaks at 321 and 418 °C are attributed to the hemicellulose and lignin losses, respectively. The

peak at 80–130 °C is attributed to the dehydration of the VSW particle, CSH, and ettringite in the case of CP10VSW and CSH, ettringite in the case of CP. In the case of the CP10VSW sample, the peak at 304 °C is assigned to the decomposition of VSW, at 400–450 °C is attributed to the decomposition of  $\text{CaCO}_3$ , while that at 620–670 °C is attributed to the decarbonization of calcium carbonate, which in CP10VSW is higher than in CP. The peak corresponding to the VSW decomposition may overlap the peaks ascribed to CH decomposition since the degradation of the lignin constituent can continue up to 500 °C, which unfavorably affects the determination CH amount as important information about cement hydration [40].

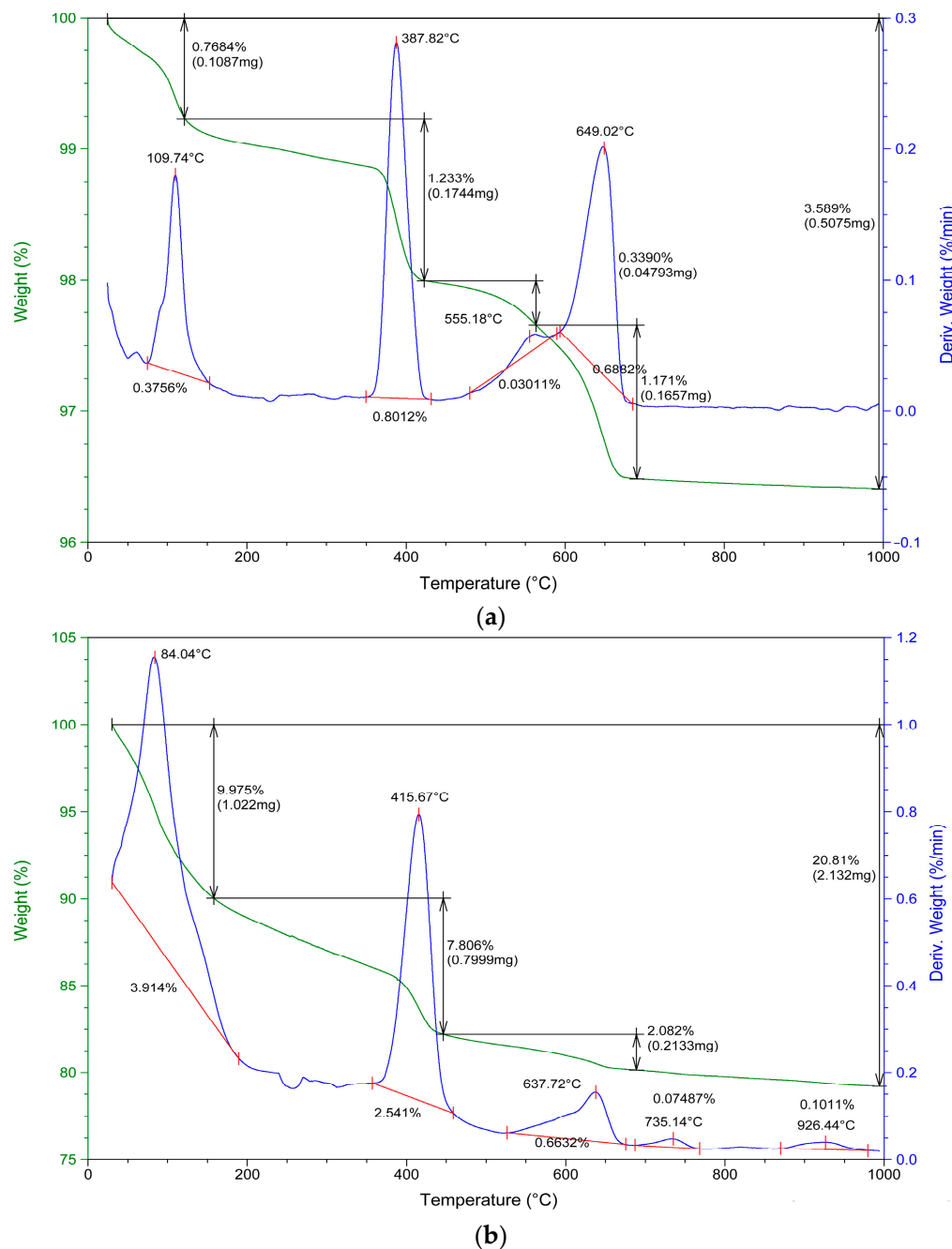
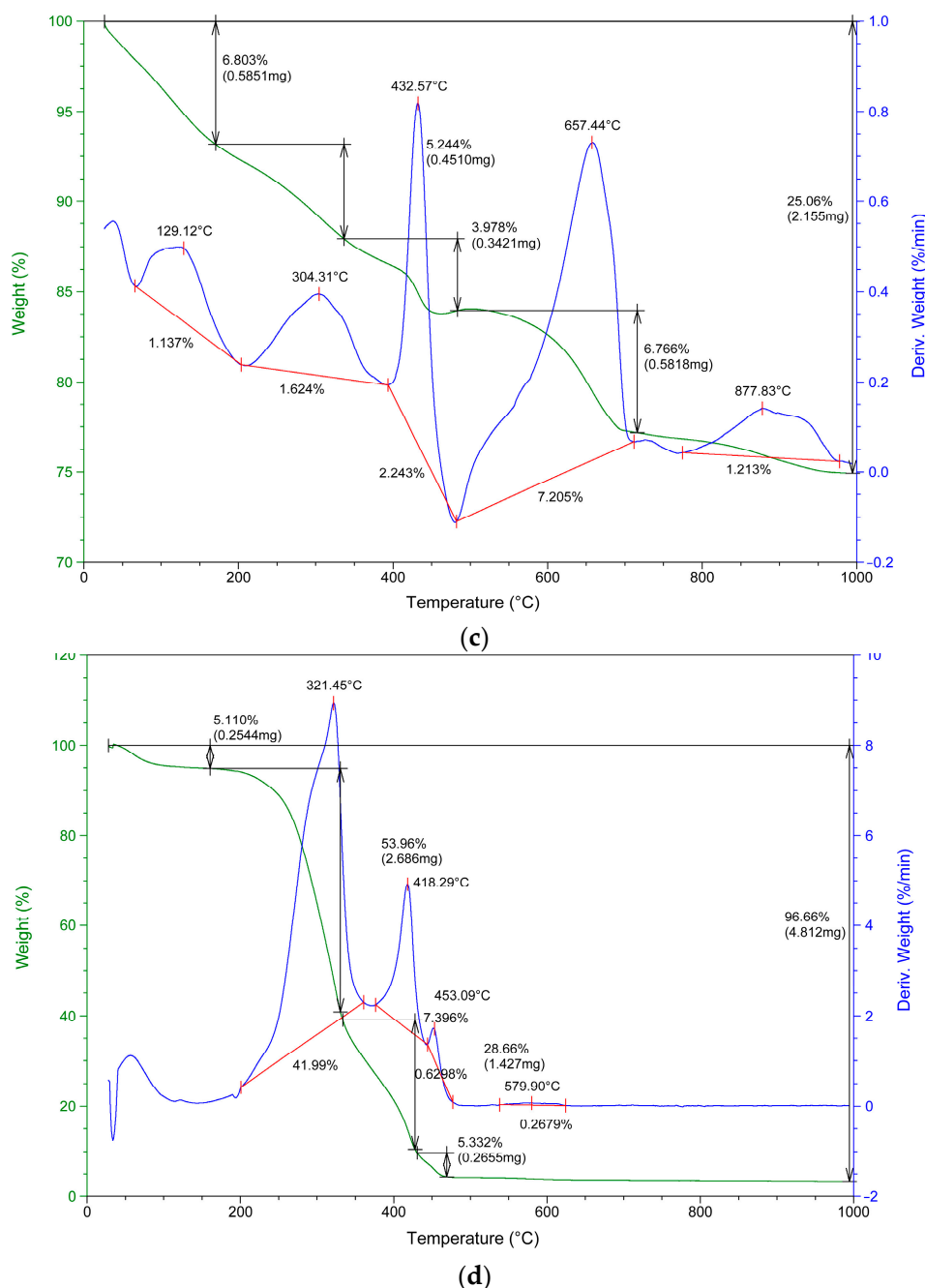


Figure 3. Cont.



**Figure 3.** TGA curve of the (a) CEM, (b) CP, (c) CP10VSW and (d) VSW samples.

#### 3.4. X-ray Diffraction (XRD)

The XRD patterns of raw materials (CEM and VSW), CP and CP10VSW samples are presented in Figure 4. The XRD pattern of VSW sample presents a broad large peak, characteristic to the amorphous state of the CEM and CP, and the CP10VSW samples display narrow peaks characteristic to the crystalline phases in the samples. XRD patterns of the CEM sample showed the existence of alite ( $C_3S$ ), belite ( $C_2S$ ), aluminate ( $C_3A$ ) and aluminate–ferrites ( $C_4AF$ ) as major crystalline phases, which correspond to the main components of the clinker and gypsum ( $CaSO_4 \cdot 2H_2O$ ). The XRD patterns of the hydration products of the investigated cement after 28 days of hydration showed the expected hydration products, including calcium hydroxide (CH), calcite ( $CaCO_3$ ), ettringite, poorly crystallized calcium silicate hydrate (CSH) and unreacted clinker phases (mainly calcium silicates). The occurrence of calcite was attributed to the partial carbonation of portlandite

by the reaction of CH with carbon dioxide from the atmosphere. The CSH products did not display distinct diffraction peaks, owing to their partial amorphous structure. Additionally, an overlapping of the diffraction peaks belonging to the hydrated and anhydrous compounds was observed. Concerning the anhydrous clinker phases, only C<sub>2</sub>S and C<sub>3</sub>S have not entirely reacted. After 28 days of hydration, the same unreacted and hydration products were observed in the CP10VSW sample. The slightly lower intensity of C<sub>2</sub>S and C<sub>3</sub>S diffraction peaks can be attributed to the charging effects and heterogeneous nucleation due to the addition of VSW content, which results in higher consumption of C<sub>2</sub>S and C<sub>3</sub>S [42]. Similar results were obtained by Lila et al. when using olive kernels and pomace for cement manufacturing [2].

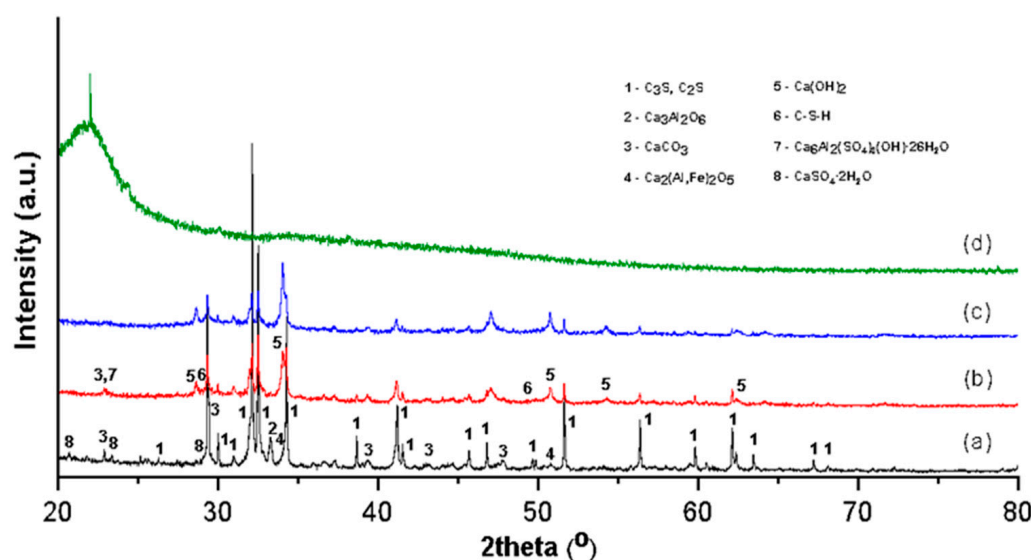


**Figure 4.** XRD patterns of (a) CEM, (b) CP, (c) CP10VSW and (d) VSW samples.

### 3.5. Scanning Electron Microscopy (SEM)

The surface topography, morphology and composition of CP and CP10VSW samples investigated by SEM-EDX are presented in Figures 5–8. Based on the analysis of the samples' topography (Figure 5), the CP sample has a porous surface with holes and small pores, while the CP10VSW sample contains fewer holes and no significant pore structure. Since pore size is one of the factors that influences the transport properties, allowing the harmful matter to pass into the cement's inner volume [43], several measurements were carried out to identify the type of pore present in the samples (Figure 6). According to the literature [43], four types of pores can be encountered in cement: gel pores (<10 nm), small capillary pores (10–100 nm), large capillary pores (100–1000 nm) and air holes (>several  $\mu\text{m}$ ). The size of cement pores is directly influenced by the preparation technique (air pores), the water content, and the hydration process of cement grains (gel and capillary pores). In the hydration process, the pore space between cement particles is gradually filled by hydration products reducing the pore size [44]. In the studied sample, the pores' radius measured for the CP sample varies in 28.96–307.14  $\mu\text{m}$  corresponding to air holes, while for CP10VSW sample, the pores' radius varies between 2.99–5.86  $\mu\text{m}$ , values which are closer to large capillary pores values. The obtained results suggest a better hydration process in the case of CP10VSW compared with the CP sample.

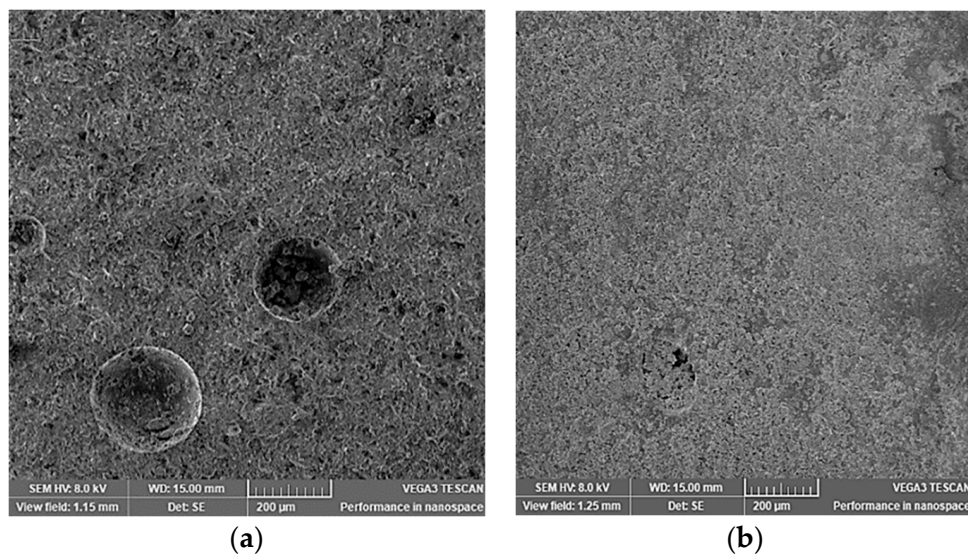


**Figure 5.** SEM images of (a) CP and (b) CP10VSW samples surface topography.

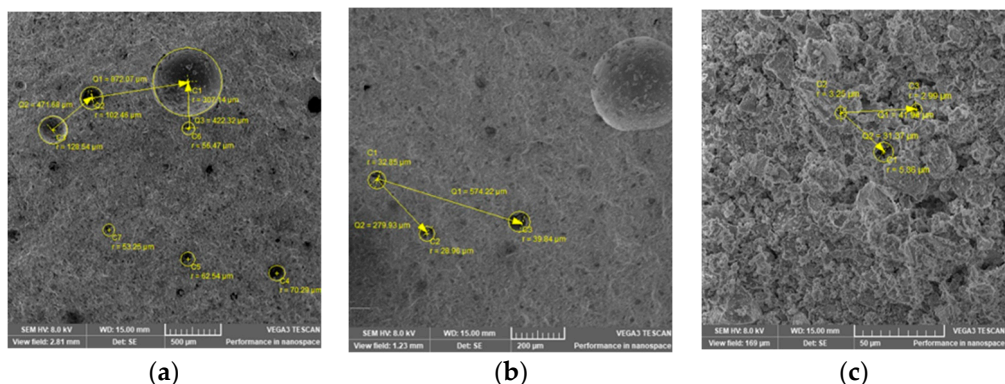


**Figure 6.** Pores structure of (a) and (b) CP and (c) CP10VSW samples.

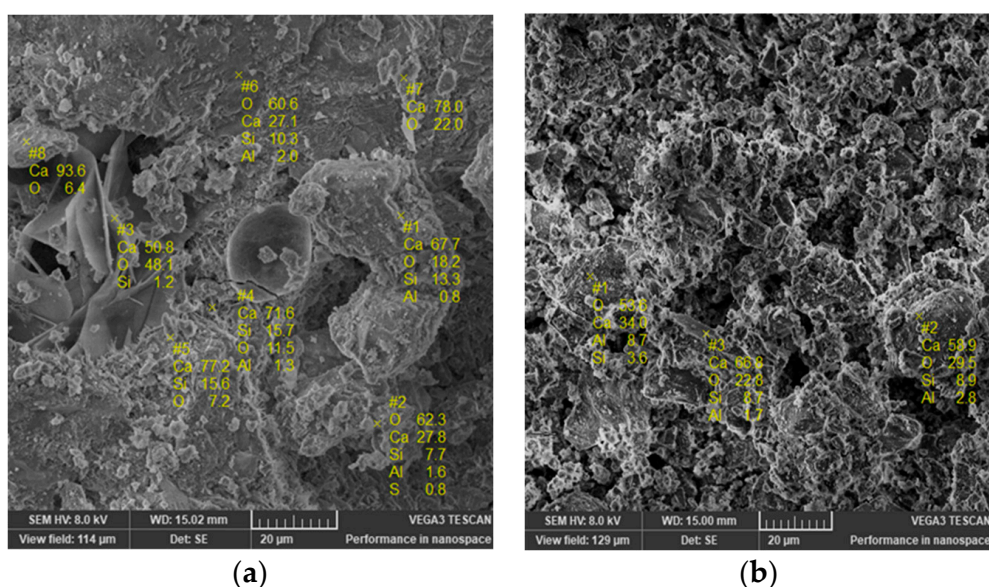


**Figure 7.** Surface topography and morphology of (a) CP and (b) CP10VSW samples at high magnification.

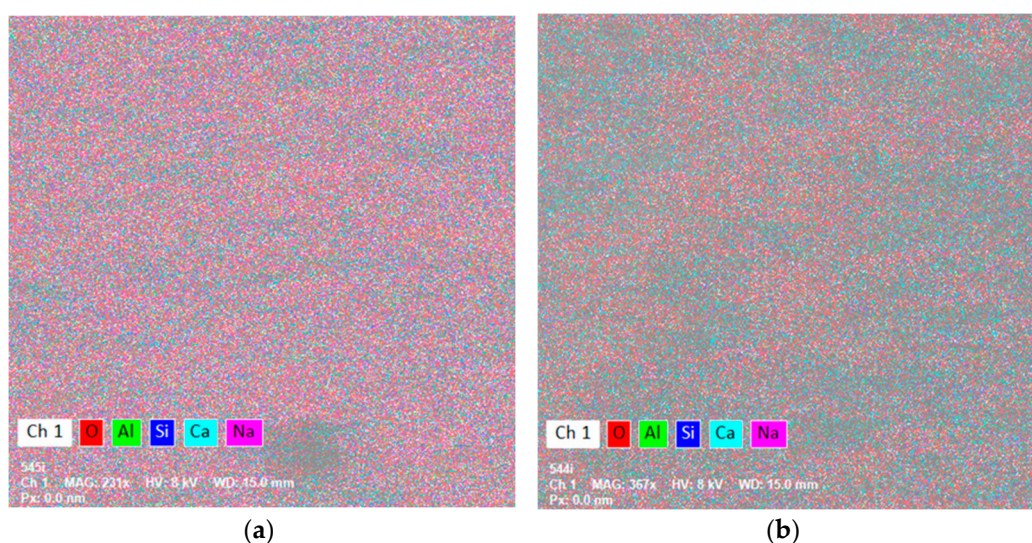


**Figure 8.** Surface mapping of (a) CP and (b) CP10VSW samples at high magnification.

The surface topography and morphology of CP and CP10VSW at high magnification can be observed in Figure 7. The figures show various formations in CP, including CH, CSH and calcium aluminosilicate, whereas only calcium aluminosilicate phases are observed in CP10VSW.

EDX was used to map the surface of the investigated samples. The maps acquired are displayed in Figure 8 and the results are presented in Table 2. The CP10VSW map shows multiple agglomerations of Ca-based phases compared to the CP map. According to the literature, the Ca/Si ratio of CSH in neat Portland cement pastes varies from ~1.2 to ~2.3 while the Ca/(Si+Al) ratio of CSH in cement-slag pastes varies from ~0.7 to ~2.4 [45]. The results presented in Table 1 reveal that both ratios are higher in the case of CP10VSW compared to CP and higher than the values presented above. These results suggest that the introduction of 10% vine shoot waste modifies the surface structure of the obtained cement by favoring the formation of Ca-based phases, such as CH and  $\text{CaCO}_3$ .

**Table 2.** Element concentrations (%) in CP and CP10VSW samples on the surface.

Sample	O	Ca	Si	Al	Na	Ca/Si	Ca/(Si + Al)
CP	53.30	35.05	8.51	1.73	1.43	<b>4.17</b>	<b>6.42</b>
CP10VSW	49.90	44.07	4.70	1.05	0.29	<b>9.37</b>	<b>32.83</b>

### 3.6. Fourier-Transform Infrared (FT-IR) Spectroscopy

The FT-IR spectra of raw materials (CEM and VSW), CP and CP10VSW samples are presented in Figure 9. The FT-IR spectra (Figure 9) of CEM show the presence of silicates, as suggested by the bands at  $\sim 930\text{ cm}^{-1}$  attributed to Si-O asymmetric stretching vibration, at  $\sim 522\text{ cm}^{-1}$  attributed to Si-O out-of-plane bending vibration and by the shoulder at  $\sim 461\text{ cm}^{-1}$  attributed to Si-O in-plane bending vibration. As well as the specific bands for silicates, there were specific bands detected for the S-O stretching ( $\sim 1154\text{ cm}^{-1}$ ) and bending ( $\sim 604\text{ cm}^{-1}$ ) vibration in the  $\text{SO}_4^{2-}$  group; the asymmetric stretching ( $\sim 1434\text{ cm}^{-1}$ ) and the out-of-plane bending ( $\sim 884\text{ cm}^{-1}$ ) vibration of the  $\text{CO}_3^{2-}$  group as well as the bands specific for -OH group stretching ( $\sim 3660\text{ cm}^{-1}$ ) and in water ( $\sim 3420$  and  $\sim 1622\text{ cm}^{-1}$ ) [29]. The FT-IR spectra of the CP confirms the formation of cement hydration products: calcium silicate hydrate gel (CSH) and CH [46]. Following the hydration, the blue shift of specific bands for silicates from  $929\text{ cm}^{-1}$  to  $974\text{ cm}^{-1}$  was noticed, confirming the polymerization of silicates and the formation of the calcium silicate hydrate gel [46,47]. The Si-O bond peak also suffers a change in profile after the hydration. The increase of the bands specific to carbonates and to water indicates the carbonation process

that appears during hydration. The FT-IR spectra of CP10VSW are similar to that of CP, calcium silicate hydrate gel (CSH) and CH are present, except for a small peak that appears at  $\sim 2940\text{ cm}^{-1}$  and is specific to -CH stretching vibration in the VSW. The FT-IR spectra of VSW show the absorption peaks specific to the cellulosic components of the vegetal fibers: -OH groups at  $\sim 3330\text{ cm}^{-1}$ , -CH groups in saturated alkane chains at  $\sim 1370$ ,  $\sim 2923$  and  $\sim 2855\text{ cm}^{-1}$ , C=O group at  $\sim 1740\text{ cm}^{-1}$ , C-O groups at  $\sim 1042\text{ cm}^{-1}$  and Si-O groups at  $\sim 594\text{ cm}^{-1}$  [47].

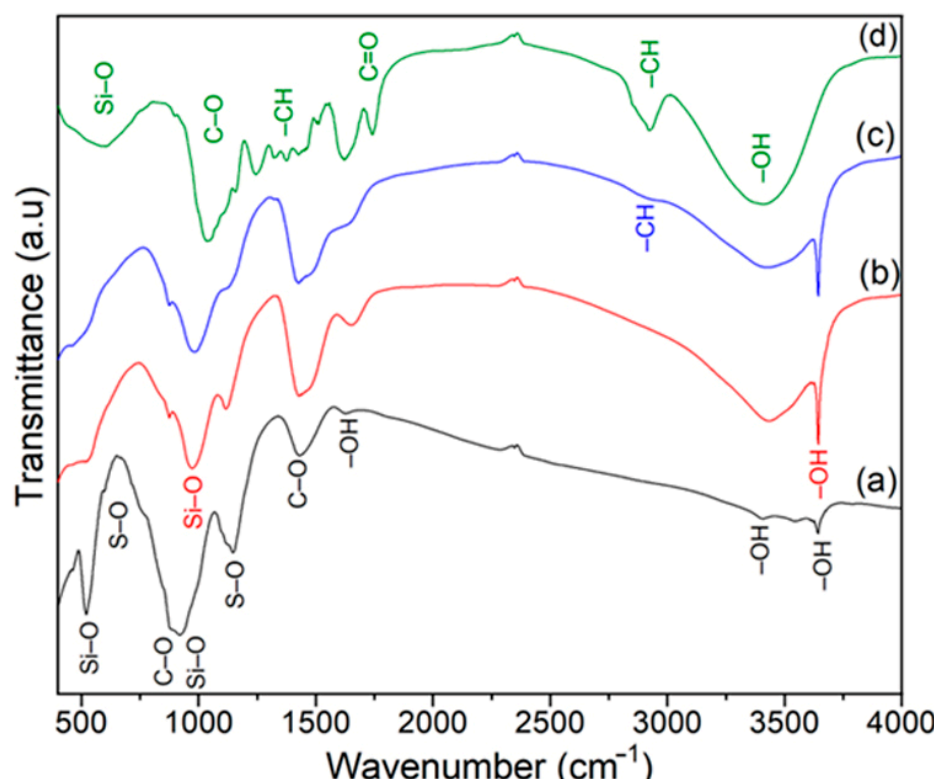


**Figure 9.** FT-IR spectra of (a) CEM, (b) CP, (c) CP10VSW, (d) VSW samples.

### 3.7. Nuclear Magnetic Resonance (NMR) Spectroscopy

The NMR spectra of raw materials (CEM and VSW), CP and CP10VSW samples are presented in Figures 10 and 11. NMR spectroscopy allows recording signals for both amorphous and crystalline parts of the investigated samples. In hydrated cement, the amorphous part consists mainly of the CSH phase, which gives the hardened cement paste mechanical strength. The  $^{27}\text{Al}$  and  $^{29}\text{Si}$  MAS NMR spectra for raw materials (CEM and VSW), CP, and CP10VSW samples are presented in Figures 10 and 11, respectively. The  $^{27}\text{Al}$  MAS NMR spectra recorded for the CEM sample show two spectral lines: at 80 ppm, attributed to the aluminate ( $\text{C}_3\text{A}$ ) and at 10 ppm, attributed to the aluminate-ferrites ( $\text{C}_4\text{AF}$ ) [48,49]. The signal from 80 ppm corresponds to the Al atoms present in the tetrahedral environment of oxygen atoms  $\text{Al}^{(\text{IV})}$ . At about 10 ppm, the signal corresponds to the aluminum atoms present in the octahedral environment of oxygen atoms  $\text{Al}^{(\text{VI})}$  [48]. VSW does not show any peak using  $^{27}\text{Al}$  MAS NMR spectroscopy. The  $^{27}\text{Al}$  MAS NMR spectra of the CP sample show the absence of aluminate and the presence of trisulphoaluminate at 13 ppm and monosulphoaluminate at 10 ppm [50]. In the presence of vine shoot waste in cement paste, the peak attributed to trisulphoaluminate does not appear and the peak attributed to monosulphoaluminate is present.

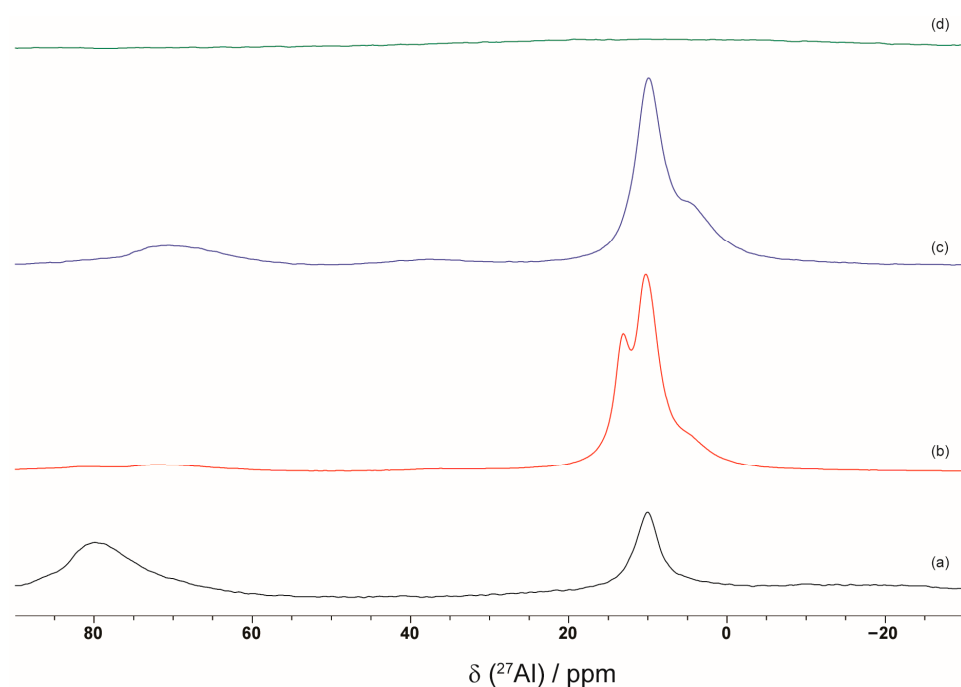


**Figure 10.**  $^{27}\text{Al}$  MAS NMR spectra of (a) CEM, (b) CP, (c) CP10VSW and (d) VSW samples.

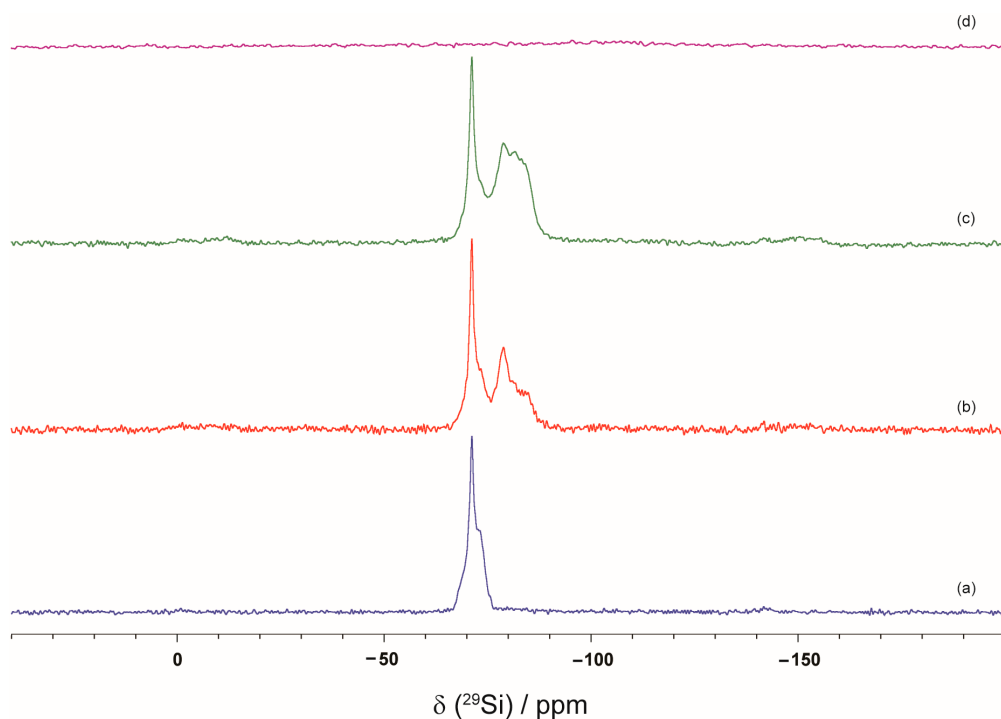


**Figure 11.**  $^{29}\text{Si}$  MAS NMR spectra of (a) CEM, (b) CP, (c) CP10VSW and (d) VSW samples.

The  $^{29}\text{Si}$  MAS NMR spectra recorded for the CEM sample show a broad spectral line between the  $-66$  to  $-77$  ppm attributed to the alite ( $\text{C}_3\text{S}$ ) and belite ( $\text{C}_2\text{S}$ ) primary phase [41]. VSW does not show any peak in the  $^{29}\text{Si}$  MAS spectra. The different structures of the CSH from CP and CP10VSW are associated with broad spectral lines ranging between  $-75$  to  $-95$  ppm and  $-66$  to  $-78$  ppm corresponding to the unhydrated clinker (alite and belite) [51,52]. CP and CP10VSW samples contain Si atoms in a tetrahedral environment of oxygen atoms. The spectral line from  $-75$  to  $-90$  ppm corresponds with one to two linked

silicon tetrahedra Q<sup>1</sup> and Q<sup>2</sup> structural elements [52]. The presence of vine shoot waste results in a higher number of different structures of CSH.

#### 4. Conclusions

This study aimed to obtain an innovative material with 10 wt.% vine shoot waste and to investigate the influence of vine shoot waste in cement paste. (i) SEM showed a compact structure of the CP10VSW sample, containing few holes and no significant pore structure; moreover, the vine shoot waste favored the formation of Ca-based phases of hydration products on the sample's surface; (ii) FT-IR spectra of CP10VSW and CP samples were similar, the presence of vine shoot waste being confirmed by the peak at ~2940 cm<sup>-1</sup> characteristic to -CH stretching vibration; (iii) TGA showed higher decarbonization of calcium carbonate in CP10VSW than in CP sample; (iv) XRD displayed lower intensity of C<sub>2</sub>S and C<sub>3</sub>S diffraction peaks due to the presence of vine shoot waste in CP10VSW and (v) <sup>27</sup>Al MAS NMR spectra revealed higher monosulphoaluminate amounts, while the <sup>29</sup>Si MAS NMR spectra showed an increased CSH structure in CP10VSW sample. The obtained results confirmed the formation of a high amount of hydration products when adding 10 wt.% vine shoot waste to the cement paste, leading to a more dense and compact cement paste with improved thermal stability and structural properties. The obtained cement-based composite containing 10 wt.% vine shoot waste can be a potential candidate for developing innovative materials for the construction sector.

**Author Contributions:** Conceptualization, D.A.S., C.R. and L.D.; methodology, D.A.S. and L.S.; investigation, D.A.S., E.K., L.S., E.A.L., D.S., X.F., M.D. and O.C.; writing—original draft preparation, D.A.S., L.S., E.A.L., D.S., X.F., M.D. and O.C.; writing—review and editing, D.A.S., E.K. and O.C.; visualization, D.A.S. and O.C.; supervision, C.R. and L.D.; project administration, D.A.S.; funding acquisition, D.A.S. All authors have read and agreed to the published version of the manuscript.

**Funding:** This work was supported by a grant of the Ministry of Research, Innovation and Digitalization within PNCDI III, project number PN-III-P1-1.1-PD-2021-0198 (LIGNOCM).

**Institutional Review Board Statement:** Not applicable.

**Informed Consent Statement:** Not applicable.

**Conflicts of Interest:** The authors declare no conflict of interest.

#### References

- Pop, A.; Ardelean, I. Monitoring the size evolution of capillary pores in cement paste during the early hydration via diffusion in internal gradients. *Cem. Concr. Res.* **2015**, *77*, 76–81. [[CrossRef](#)]
- Lila, K.; Belaadi, S.; Solimando, R.; Zirour, F.R. Valorisation of organic waste: Use of olive kernels and pomace for cement manufacture. *J. Clean. Prod.* **2020**, *277*, 123703. [[CrossRef](#)]
- Nodehi, M.; Taghvaei, V.M. Sustainable concrete for circular economy: A review on use of waste glass. *Glass Struct. Eng.* **2022**, *7*, 3–22. [[CrossRef](#)]
- EN 197-1/2011; Cement—Part 1: COMPOSITION, Specifications and Conformity Criteria for Common Cements. Available online: <https://standards.iteh.ai/catalog/standards/cen/64d327b1-d5ac-45e3-8b04-fafec9e0698e/en-197-1-2011#:~{:text=This%20European%20Standard%20defines%20and,furnace%20cements%20and%20their%20constituents}> (accessed on 25 April 2022).
- Kosmatka, S.H.; Kerkhoff, B.; Panarese, W.C. *Design and Control of Concrete Mixtures*, 14th ed.; Portland Cement Association: Skokie, IL, USA, 2002; pp. 21–56.
- Usman, M.; Khan, A.Y.; Farooq, S.H.; Hanif, A.; Tang, S.; Khushnood, R.A.; Rizwan, S.A. Eco-friendly self-compacting cement pastes incorporating wood waste as cement replacement: A feasibility study. *J. Clean. Prod.* **2018**, *190*, 679–688. [[CrossRef](#)]
- Bergeron, F.C. Energy and climate impact assessment of waste wood recovery in Switzerland. *Biomass Bioenerg.* **2016**, *94*, 245–257. [[CrossRef](#)]
- Faraca, G.; Tonini, D.; Astrup, T.F. Dynamic accounting of greenhouse gas emissions from cascading utilisation of wood waste. *Sci. Total Environ.* **2019**, *651*, 2689–2700. [[CrossRef](#)]
- Jamora, J.B.; Emily, S.; Gudia, L.; Woo, A.; Giduquio, M.B.; Wilbert, J.; Orilla, A.; Loretero, M.E. Potential reduction of greenhouse gas emission through the use of sugarcane ash in cement-based industries: A case in the Philippines. *J. Clean. Prod.* **2019**, *239*, 118072. [[CrossRef](#)]
- Ramage, M.H.; Burridge, H.; Busse-Wicher, M.; Fereday, G.; Reynolds, T.; Shah, D.U.; Wu, G.; Yu, L.; Fleming, P.; Densley-Tingley, D.; et al. The wood from the trees: The use of timber in construction. *Renew. Sustain. Energy Rev.* **2017**, *68*, 333–359. [[CrossRef](#)]

11. Ma, S.; Zhang, Z.; Liu, X.; Li, Y.; Zeng, Q.; Zhang, W. Reuse of red mud in magnesium potassium phosphate cement: Reaction mechanism and performance optimization. *J. Build. Eng.* **2022**, *16*, 105290. [[CrossRef](#)]
12. Nascimento, E.S.S.; de Souza, P.C.; de Oliveira, H.A.; Junior, C.M.M.; de Oliveira Almeida, V.G.; de Melo, F.M.C. Soil-cement brick with granite cutting residue reuse. *J. Clean. Prod.* **2021**, *321*, 129002. [[CrossRef](#)]
13. Geng, C.; Wu, X.; Yao, X.; Wang, C.; Mei, Z.; Jiang, T. Reusing waste glass powder to improve the strength stability of cement at HTHP. *J. Pet. Sci. Eng.* **2022**, *213*, 110394. [[CrossRef](#)]
14. Kupwade-Patil, K.; Palkovic, S.D.; Bumajdad, A.; Soriano, C.; Büyüköztürk, O. Use of silica fume and natural volcanic ash as a replacement to Portland cement: Micro and pore structural investigation using NMR, XRD, FTIR and X-ray microtomography. *Constr. Build. Mater.* **2018**, *158*, 574–590. [[CrossRef](#)]
15. Karade, S.R. Cement-bonded composites from lignocellulosic wastes. *Constr. Build. Mater.* **2010**, *24*, 1323–1330. [[CrossRef](#)]
16. Gupta, S.; Kua, H.W.; Low, C.Y. Use of biochar as carbon sequestering additive in cement mortar. *Cem. Concr. Compos.* **2018**, *87*, 110–129. [[CrossRef](#)]
17. Savastano, H., Jr.; Warden, P.G.; Coutts, R.S.P. Mechanically pulped sisal as reinforcement in cementitious matrices. *Cem. Concr. Compos.* **2003**, *25*, 311–319. [[CrossRef](#)]
18. Scatolino, M.V.; Silva, D.W.; Mendes, R.F.; Mendes, L.M. Use of maize cob for production of particleboard. *Cienc. Agropecuaria* **2013**, *37*, 330–337. [[CrossRef](#)]
19. Tonoli, G.H.D.; Almeida, A.E.F.S.; Bassa, M.A.; Pereira-Da-Silva, A.; Oyakawa, D.; Savastano, H., Jr. Surface properties of eucalyptus pulp fibres as reinforcement of cement-based composites. *Holzforschung* **2010**, *64*, 595–601. [[CrossRef](#)]
20. Savastano, H., Jr.; Fiorelli, J.; dos Santos, S.F. *Sustainable and Nonconventional Construction Materials Using Inorganic Bonded Fiber Composites*; Elsevier: Amsterdam, The Netherlands; Duxford, UK, 2017; pp. 4–16.
21. Wong, V.; Chan, K.W.; Kwan, A.K.H. Applying theories of particle packing and rheology to concrete for sustainable development. *Organ. Technol. Manag. Constr. Int. J.* **2013**, *5*, 841855. [[CrossRef](#)]
22. Vance, K.; Kumar, A.; Sant, G.; Neithalath, N. The rheological properties of ternary binders containing Portland cement, limestone, and metakaolin or fly ash. *Cem. Concr. Res.* **2013**, *52*, 196–207. [[CrossRef](#)]
23. Lekshmi, M.S.; Vishnudas, S.; Anil, K.R. Lignocellulosic materials as reinforcement and replacement for binders in masonry mortar. *Constr. Build. Mater.* **2021**, *282*, 122607. [[CrossRef](#)]
24. Manzone, M.; Paravidino, E.; Bonifacino, G.; Balsari, P. Biomass availability and quality produced by vineyard management during a period of 15 years. *Renew. Energy* **2016**, *99*, 465–471. [[CrossRef](#)]
25. Pizzi, A.; Pedretti, E.F.; Duca, D.; Rossini, G.; Mengarelli, C.; Ilari, A.; Mancini, M.; Toscano, G. Emissions of heating appliances fuelled with agropellet produced from vine pruning residues and environmental aspects. *Renew. Energy* **2018**, *121*, 513–520. [[CrossRef](#)]
26. Zanetti, M.; Brandedet, B.; Marini, D.; Sgarbossa, A.; Giorio, C.; Badocco, D.; Tapparo, A.; Grigolato, S.; Rogau, C.; Rogau, Y.; et al. Vineyard pruning residues pellets for use in domestic appliances: A quality assessment according to the EN ISO 17225. *J. Agric. Eng. Res.* **2017**, *48*, 99. [[CrossRef](#)]
27. El Achaby, M.; El Miri, N.; Hannache, H.; Gmouh, S.; Youcef, H.B.; Aboulkas, A. Production of cellulose nanocrystals from vine shoots and their use for the development of nanocomposite materials. *Int. J. Biol. Macromol.* **2018**, *117*, 592–600. [[CrossRef](#)]
28. Ntalos, G.A.; Grigoriou, A.H. Characterization and utilisation of vine prunings as a wood substitute for particleboard production. *Ind. Crops Prod.* **2002**, *16*, 59–68. [[CrossRef](#)]
29. Muñoz, P.; Mendivil, M.A.; Letelier, V.; Morales, M.P. Thermal and mechanical properties of fired clay bricks made by using grapevine shoots as pore forming agent. Influence of particle size and percentage of replacement. *Constr. Build. Mater.* **2019**, *224*, 639–658. [[CrossRef](#)]
30. Teramoto, Y.; Lee, S.-H.; Endo, T. Pretreatment of woody and herbaceous biomass for enzymatic saccharification using sulfuric acid-free ethanol cooking. *Bioresour. Technol.* **2008**, *99*, 8856–8863. [[CrossRef](#)]
31. EN ISO 18134-3/2015; Solid Biofuels—Determination of Moisture Content—Oven Dry Method—Moisture in General Analysis Sample. Available online: <https://www.iso.org/standard/61637.html> (accessed on 25 April 2022).
32. ASTM E1755-01/2020; Standard Test Method for Ash in Biomass. Available online: <https://www.astm.org/e1755-01r20.html> (accessed on 25 April 2022).
33. Cadar, O.; Senila, M.; Hoaghia, M.-A.; Scurtu, D.; Miu, I.; Levei, E.A. Effects of thermal treatment on natural clinoptilolite-rich zeolite behavior in simulated biological fluids. *Molecules* **2020**, *25*, 2570. [[CrossRef](#)]
34. ASTM C114/2018; Standard Test Methods for Chemical Analysis of Hydraulic Cement. Available online: <https://www.astm.org/c114-18.html> (accessed on 25 April 2022).
35. Senila, L.; Neag, E.; Torok, I.; Cadar, O.; Kovacs, E.; Tenu, I.; Roman, C. Vine shoots waste—new resources for bioethanol production. *Rom. Biotechnol. Lett.* **2020**, *25*, 1253–1259. [[CrossRef](#)]
36. EN 196-2/2013; Methods of Testing Cement—Part 2: Chemical Analysis of Cement. Available online: <https://standards.iteh.ai/catalog/standards/cen/47283941-90a2-43dc-8b2c-dea6208712a6/en-196-2-2013> (accessed on 25 April 2022).
37. Kong, X.-M.; Liua, H.; Lu, Z.-B.; Wang, D.-M. The influence of silanes on hydration and strength development of cementitious systems. *Cem. Concr. Res.* **2015**, *67*, 168–178. [[CrossRef](#)]
38. Javed, M.H.; Sikandar, M.A.; Ahmad, W.; Bashir, M.T.; Alrowais, R.; Wadud, M.B. Effect of various biochars on physical, mechanical, and microstructural characteristics of cement pastes and mortars. *J. Build. Eng.* **2022**, *57*, 104850. [[CrossRef](#)]

39. Sousa, M.I.C.; da Silva Rego, J.H. Effect of nanosilica/metakaolin ratio on the calcium alumina silicate hydrate (C-A-S-H) formed in ternary cement pastes. *J. Build. Eng.* **2021**, *38*, 102226. [[CrossRef](#)]
40. Çavdar, A.D.; Yel, H.; Torun, S.B. Microcrystalline cellulose addition effects on the properties of wood cement board. *J. Build. Eng.* **2022**, *48*, 103975. [[CrossRef](#)]
41. Zeng, Q.; Li, K.; Fen-Chong, T.; Dangla, P. Determination of cement hydration and pozzolanic reaction extents for fly-ash cement pastes. *Constr. Build. Mater.* **2012**, *27*, 560–569. [[CrossRef](#)]
42. Xu, G.; Tian, Q.; Miao, J.; Liu, J. Early-age hydration and mechanical properties of high volume slag and fly ash concrete at different curing temperatures. *Constr. Build. Mater.* **2017**, *149*, 367–377. [[CrossRef](#)]
43. Song, Y.; Zhou, J.; Bian, Z.; Dai, G. Pore structure characterization of hardened cement paste by multiple methods. *Adv. Mater. Sci. Eng.* **2019**, *2019*, 3726953. [[CrossRef](#)]
44. Liu, C.; Zhang, M.; Fang, G.; Bai, Y.; Zhang, Y. *Modelling of capillary pore structure evolution in portland cement pastes based on irregular-shaped cement particles. Durability of Concrete Structures: Sixth International Conference—ICDCS 2018*, 1st ed.; Basheer, P.A.M., Ed.; Whittles Publishing: Caithness, UK, 2018.
45. Richardson, I.G. The nature of C-S-H in hardened cements. *Cem. Concr. Res.* **1999**, *29*, 1131–1147. [[CrossRef](#)]
46. Bhat, P.A.; Debnath, N.C. Study of structures and properties of silica-based clusters and its application to modeling of nanostructures of cement paste by DFT methods. *IOP Conf. Ser. Mater. Sci. Eng.* **2013**, *43*, 012001. [[CrossRef](#)]
47. Liu, Z.; Hana, C.; Li, Q.; Li, X.; Zhou, H.; Song, X.; Zu, F. Study on wood chips modification and its application in wood-cement composites. *Case Stud. Constr. Mater.* **2022**, *17*, e01350. [[CrossRef](#)]
48. Li, J.; Liu, X.; Yang, Q.; Hou, D.; Hu, X.; Ye, Q.; Wang, D.; Ding, Q. Characterization of fly ash-cement paste and molecular structure in the presence of seawater by  $^{27}\text{Al}$  and  $^{29}\text{Si}$  MAS NMR spectroscopy. *Constr. Build. Mater.* **2020**, *262*, 120823. [[CrossRef](#)]
49. Walkley, B.; Provis, J.L. Solid-state nuclear magnetic resonance spectroscopy of cements. *Mater. Today Adv.* **2019**, *1*, 100007. [[CrossRef](#)]
50. Martinia, F.; Tonellic, M.; Geppia, M.; Ridic, F.; Borsacchia, S.; Caluccia, L. Hydration of  $\text{MgO}/\text{SiO}_2$  and Portland cement mixtures: A structural investigation of the hydrated phases by means of X-ray diffraction and solid state NMR spectroscopy. *Cem. Concr. Res.* **2017**, *102*, 60–67. [[CrossRef](#)]
51. Kunther, W.; Dai, Z.; Skibsted, J. Thermodynamic modeling of hydrated white Portland cement–metakaolin–limestone blends utilizing hydration kinetics from  $^{29}\text{Si}$  MAS NMR spectroscopy. *Cem. Concr. Res.* **2016**, *86*, 29–41. [[CrossRef](#)]
52. Mazur, A.; Tolstoy, P.; Sotiriadis, K.  $^{13}\text{C}$ ,  $^{27}\text{Al}$  and  $^{29}\text{Si}$  NMR Investigation of the hydration kinetics of portland-limestone cement pastes containing  $\text{CH}_3\text{COO}^- \text{R}^+$  ( $\text{R}=\text{H}$  or  $\text{Na}$ ) Additives. *Materials* **2022**, *15*, 2004. [[CrossRef](#)] [[PubMed](#)]

**Disclaimer/Publisher’s Note:** The statements, opinions and data contained in all publications are solely those of the individual author(s) and contributor(s) and not of MDPI and/or the editor(s). MDPI and/or the editor(s) disclaim responsibility for any injury to people or property resulting from any ideas, methods, instructions or products referred to in the content.